How important is the dose rate sensitivity of 2D and 3D radiation dosimeters?

IOP Conf. Series: Journal of Physics: Conf. Series **1305** (2019) 012059 doi:10.1088/1742-6596/1305/1/012059

How important is the dose rate sensitivity of 2D and 3D radiation dosimeters?

Yves De Deene
School of Engineering, Macquarie University, North Ryde, Sydney, Australia

E-mail: Yves.DeDeene@mq.edu.au

Abstract. Several kinds of chemical 3D radiation dosimeters have been fabricated to acquire the dose distribution in clinical radiotherapy. A legitimate concern with every new dosimeter is its dose rate dependent response because, the dose rate in each point of the phantom during a clinical treatment is unknown. Unfortunately, many 3D dosimeters have shown some degree of dose rate dependence. In practice, radiation dosimeters are mostly calibrated using a calibration curve that is obtained by irradiating calibration vials with different doses but using a fixed dose rate. Therefore, when applying a dose calibration to an experimentally obtained dose distribution, a deviation between the measured dose distribution and the actual dose distribution can be expected. In this computational study, the effect of a dose rate dependent dosimeter response on a theoretical dose distribution has been investigated. In order to compare the effect of dose rate, a gamma evaluation is performed between the predefined dose distribution and the dose distribution that is affected by a dose rate dependent radiation response. It is found that a dose rate difference of -10%, results in a gamma pass rate of 100% in the 3D dose distribution.

1. Introduction

Experimental 3D dosimeters show some degree of dose rate dependence, but the dose rate dependence varies significantly between the different dosimeters. The dose rate dependence of 3D radiation dosimeters was extensively studied for some polymer gel dosimeters [1], PRESAGE [2] and Flexydos3D [3] and for different imaging systems including MRI, optical CT and X-ray CT. However, the dose rate dependence has not been documented for all gel systems.

Dose rate and temperature effects on a dose distribution need to be assessed relative to the dose range in which the dosimeter is used. If the imaged property is labeled ψ, the dose sensitivity of the dosimeter is $\frac{\partial \psi}{\partial D}$ and the change of the dose sensitivity with dose rate is $\frac{\partial}{\partial \dot{D}}\left(\frac{\partial \psi}{\partial D}\right)$ where $\dot{D}$ is the dose rate mostly expressed in units of (cGy/min). Temperature may affect both the reading of a non-irradiated sample ($\psi_0 = \psi(D = 0\ Gy)$) and the dose sensitivity ($\frac{\partial \psi}{\partial D}$). The imaged property ψ can be the NMR spin-lattice relaxation rate (R_1 (s^{-1})), the NMR spin-spin relaxation rate (R_2 (s^{-1})), optical density (OD), X-ray CT number (CT_{Number} (HU)). From figure 1, it can be easily seen, that if a dosimeter is calibrated using samples at a fixed dose rate ($\dot{D}_{cal}$), the derived dose (D_{meas}) in any point of the dosimeter will be:

$$D_{meas} = \left(\frac{\left(\frac{\partial \psi}{\partial D}\right)_{\dot{D}}}{\left(\frac{\partial \psi}{\partial D}\right)_{\dot{D}_{cal}}} \right) \cdot D \qquad (1)$$

where $\left(\frac{\partial\psi}{\partial D}\right)_{\dot{D}}$ is the dose sensitivity for a dose rate $\dot{D}$ received in the corresponding pixel of the dosimeter, $\left(\frac{\partial\psi}{\partial D}\right)_{\dot{D}_{cal}}$ is the dose sensitivity for the dose rate at which the calibration was performed $\dot{D}_{cal}$.
In a first order approximation, the dose response curves can be considered as linear and the dependence on dose rate can also be considered as linear:

$$\left(\frac{\partial\psi}{\partial D}\right)_{\dot{D}} = \left(\frac{\partial\psi}{\partial D}\right)_{\dot{D}_{cal}} + \frac{\partial}{\partial\dot{D}}\left(\frac{\partial\psi}{\partial D}\right)\cdot\left(\dot{D}-\dot{D}_{cal}\right)$$

Note that in an actual dosimetry experiment, every spatial point in the dosimeter phantom will have received a total dose that will be a combination of doses delivered at several different dose rates as every point consists of a superposition of several beams.

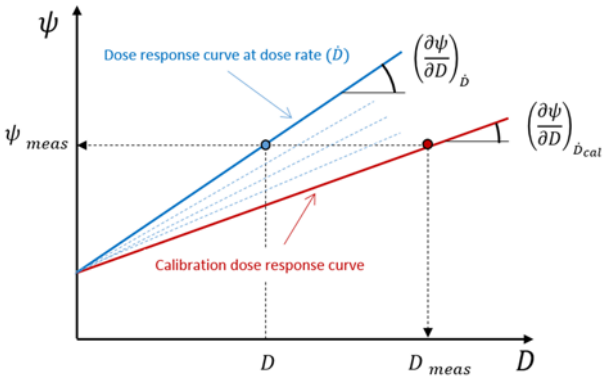

Figure 1. Illustration of the effect of calibration using calibration samples irradiated at dose rate $\dot{D}_{cal}$. With any given spatial point in the dosimeter corresponds a dose response curve (blue line) that results in a measurement ψ_{meas}. This value is converted in a 'measured' dose value D_{meas} using the calibration curve (red).

Using equation 1, the percentage dose error as a result of dose rate dependent dose response can be written as:

$$\epsilon_{\dot{D}} = \left(\frac{D_{meas}-D}{D}\right)\cdot 100\% = \left(\frac{\left(\frac{\partial\psi}{\partial D}\right)_{\dot{D}} - \left(\frac{\partial\psi}{\partial D}\right)_{\dot{D}_{cal}}}{\left(\frac{\partial\psi}{\partial D}\right)_{\dot{D}_{cal}}}\right)\cdot 100\% \qquad (2)$$

The dose rate related dose error $\epsilon_{\dot{D}}$ for a dose rate range between [50 cGy/min, 400 cGy/min] is summarized in table 1.

Table 1. Dose rate dependency and temperature dependency of some potential 3D radiation dosimeters. Literature values for dose rate dependence are (re)calculated for the dose rate range of [50 cGy/min, 400 cGy/min] by linear interpolation/extrapolation when not available. Note the big difference in dose rate dependence between the different dosimeters.

Dosimeter	Read out	$\epsilon_{\dot{D}}\vert_{50\ cGy/min}^{400\ cGy/min}$ (%)	$\frac{\partial\psi_0}{\partial T}$	$\frac{\partial}{\partial T}\left(\frac{\partial\psi}{\partial D}\right)\Big/\left(\frac{\partial\psi}{\partial D}\right)_{20\,℃}$
PAG [1]	MRI (R2)	-5 %	Nil	0.2 % K^{-1}
MAGAT [1]	MRI (R2)	-45 %	Nil	−2.1 % K^{-1}
PAGAT [1]	MRI (R2)	-2 %	Nil	0.4 % K^{-1}
Micelle Gel [2]	Optical (OD)	-32 %		0.2 % K^{-1}
PRESAGE™ [3]	Optical (OD)	-16 %	-	-
Flexydos3D [4]	Optical (OD)	-21 %	Nil	0.3 % K^{-1}
NIPAM PG [5]	X-ray CT	-12 %	-	-

Important to note is that the dose rate dependence of most 3D dosimeters is not linear, with higher dose rate dependence at lower dose rates. The values provided in table 1 are therefore only indicative.

Despite the many attempts to fabricate radiation dosimeters that exhibit minimal dose rate dependency, there is no study on how a dose rate dependent radiation response affects a clinically realistic dose distribution. In this study, we investigate the effect of a dose rate dependency of the 3D radiation dosimeter on the measured dose distribution.

2. Methods and Materials

2.1. Construction of the dose distribution

A hypothetical dose distribution is obtained by superimposing several beams from different directions on a cylindrical phantom using a coplanar beam set-up. In one part of the simulation study, the dose rate effect on the dose distributions was studied for various phantom diameters. The dose distribution was calculated by using a superposition of theoretical square radiation beams. The theoretical radiation beams are based on dose measurements acquired with an ionization chamber. Depth dose and lateral dose profiles were fitted against an in house developed physical model:

$$D\ (x,y,z)\ = D_0 \frac{sinh(\xi a(z))}{cosh(\xi x)+cosh(\xi a(z))} \cdot \frac{\sinh(\xi a(z))}{cosh(\xi y)+\cosh(\xi a(z))} \cdot \frac{SSD^2}{(z-SSD)^2}\left(e^{-\psi_p z} - e^{-\psi_e z}\right) \qquad (3)$$

where x and y are lateral directions and z is the beam direction. The origin of the coordinate system (x,y,z) is considered to coincide with the entrance point of the beam in the phantom. The first two hyperbolic factors in the equation define the lateral profile with field size a. The field size varies with depth according to $a(z) = \frac{(SSD+z)\cdot a(0)}{SSD}$. The parameter ξ accounts for the penumbra width and is derived by fitting to the ion chamber measured beam data, SSD is the source-to-surface distance and ψ_p and ψ_e are parameters that are linked to the photon and electron mass attenuation coefficients. However, they deviate from the true mass attenuation coefficients as a result of scatter contributions in the actual beam. D_0 is the dose defined at the surface of the phantom. The equation can be easily rewritten using the Tissue-Maximum Ratio (TMR). Regardless the simplified radiation model which doesn't account for any tissue inhomogeneities, we found however that an excellent fit of beam dose data was obtained against equation 1 for a range of square field sizes between 2 and 10 cm. This simplified model allowed us to quickly generate a realistic dose distribution in a cylindrical geometry with a multitude of beam configurations and phantom sizes. In this example, 2 cm × 2 cm fields were used and the output factor was taken into account in the scaling factor D_0 of equation 3. The off-axis-factor (OAF) was taken equal to 1 for simplicity.

The hyperbolic factors in equation 3 describing the lateral profiles of the beam, satisfy the property of superposition [6]:

$$\begin{aligned} P(x,a) &= \frac{\sinh\left(\xi a(z)\right)}{cosh(\xi x) + \cosh\left(\xi a(z)\right)} \\ &= \sum_{i=0}^{n-1} p[x + (2i+1)\cdot\delta, \delta] + p[x - (2i+1)\cdot\delta, \delta]\ , \quad \forall n \in \mathbb{N} \end{aligned} \qquad (4)$$

Because of this particular property of superposition, the beam was split up in n small segments with half width δ in the calculation algorithm to accommodate for the curved surface of the cylindrical phantom in the x-direction.

While this simulation comprises a simplified and fast algorithm written in MATLAB, as compared to the use of more sophisticated convolution-superposition or Monte Carlo based treatment planning

systems, it is considered not to make a significant difference on the assessment of the dose rate effect. It can be assumed that the distribution of dose values above a certain minimum dose value threshold is not significantly affected by the geometry.

2.2. The effect of dose rate dependent dose response

The effect of the dose rate dependent dose response was taken into account by considering equation 2 which can be rewritten as:

$$D_{meas} = D\ (1 + \epsilon_{\dot{D}}) \tag{5}$$

where $\epsilon_{\dot{D}}$ is dependent on the dose rate $\dot{D}(x, y, z)$ and on the dose rate $\dot{D}_{cal}$ at which the calibration is performed according to equation 2. Combining equation 1 and 2 and using the values from table 1, $\epsilon_{\dot{D}}$ can be linearized as:

$$\begin{aligned} \epsilon_{\dot{D}} &= \left(\frac{\dot{D}_{cal}}{(400\ cGy/min - 50\ cGy/min)} \cdot \epsilon_{\dot{D}}\Big|_{50\ cGy/min}^{400\ cGy/min}\right)\left(\frac{\dot{D}}{\dot{D}_{cal}} - 1\right) \\ &= \epsilon_{\dot{D}}\Big|_{0}^{\dot{D}_{cal}}\left(\frac{\dot{D}}{\dot{D}_{cal}} - 1\right) \end{aligned} \tag{6}$$

In this equation, $\epsilon_{\dot{D}}|_{0}^{\dot{D}_{cal}}$ is the dose rate dependency factor for calibrations performed at a dose rate $\dot{D}_{cal}$ for actual dose delivery at infinitely small dose rates ($\dot{D} \to 0\ cGy/\mathrm{min}$). For every single beam, the dose rate can be considered proportional to the dose. During the calculation of the dose distribution, the dose of each individual beam is stored. After the calculation of the actual dose distribution for every beam, the simulated dose incorporating a dose rate dependence is calculated for every beam using equation 6. After summing the dose rate affected dose for every beam, the simulated dose rate affected dose distribution is obtained.

After calculating the actual and the dose rate affected dose distribution, a gamma comparison is performed between the two dose distributions. The gamma pass rate is calculated for all dose values above a dose threshold of 5%.

3. Results and Discussion

The Matlab program using the beam superposition algorithm allowed to calculate dose distributions very quickly for different levels of dose rate dependence and for a multitude of different scenarios (different phantom size, number of beams and beam directions). 3D gamma evaluations were performed between the actual (theoretical) dose distribution and the dose distributions affected by the dose rate dependence.

Figure 1 shows a typical simulation of a 12 beam coplanar irradiation with square 6 MV photon beams within an arc of 250 degrees. The dose distribution of a single beam is also shown (figure 1c) that was obtained by splitting the beam in 10 beam segments along the x-direction.

A comparison between the actual and dose rate affected ('measured') dose distribution is shown in figure 2. Some groups have been using 3D dosimetry in a relative way, where the radiation dose distribution is scaled towards the maximum dose. The effect of this renormalization is illustrated in figure 2, d-f.

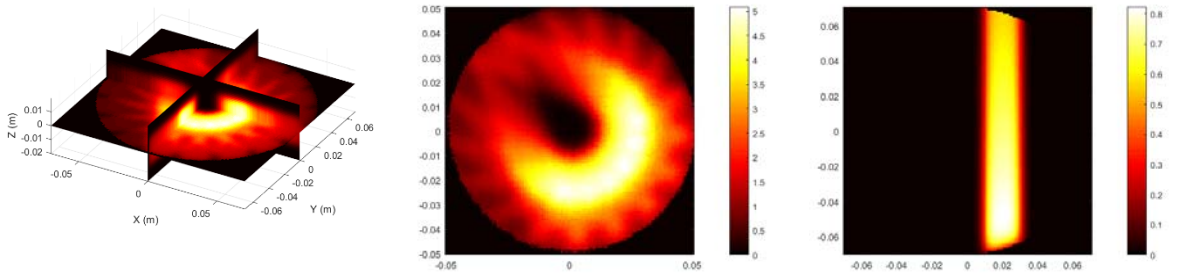

(a) **(b)** **(c)**

Figure 2. A typical simulated dose distribution in 3D (a) and in a central plane (b), for a cylindrical phantom (R = 5 cm) irradiated with 12 beams in an arc of 250 degrees. The calculated dose distribution of a single beam (2 cm × 2 cm) is also shown (c).

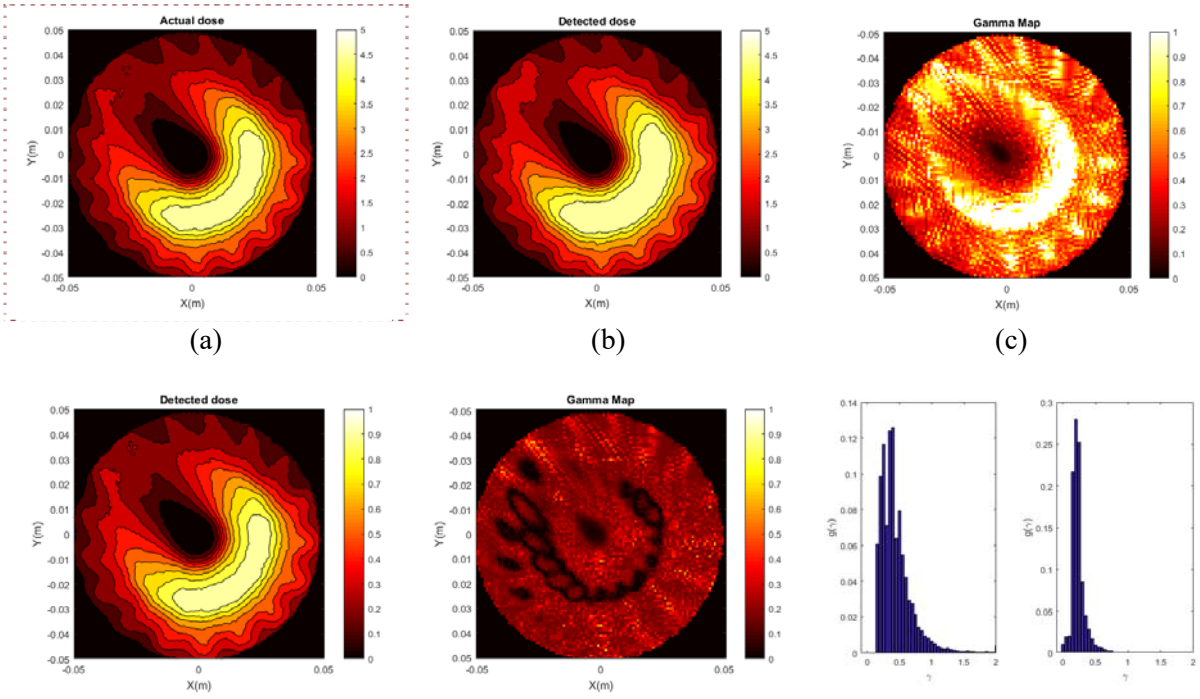

(a) (b) (c)

(d) (e) (f) (g)

Figure 3. Contour isodose plot of the computed dose distribution in the isocentric transverse plane with a 12 beam 250 degree arc (a) and corresponding computed dose distribution assuming a dose rate dependence $\epsilon_{\dot{D}}|_0^{\dot{D}_{cal}} = -20\%$ (b). The corresponding gamma map is shown in c. After renormalization of the detected dose distribution (d), the gamma map shows no values above 1 (e). Corresponding gamma value histograms are shown in f and g for absolute calibration and relative dose calibration (renormalization towards the maximum dose) respectively.

Most dosimeters exhibit a decrease in dose sensitivity with increasing dose rate. As a result, the detected dose will be overestimated if the calibration samples are irradiated at a higher dose rate. The overestimation of dose is also apparent when comparing the detected dose distribution (figure 2b) with the reference dose distribution (figure 2a). After normalization of the detected dose distribution towards the maximum dose (figure 2d), a closer agreement is found in the gamma evaluation (figure 2e, g).

Figure 3a shows the trend in gamma-pass rates as a function of dose rate dependency coefficient ($\epsilon_{\dot{D}}|_0^{\dot{D}_{cal}}$) for three different phantom radii. It is clear that the phantom radius and as a result the dose distribution has only a small effect on the gamma pass rates. Figure 3b shows the trend in gamma-pass rates as a function of dose rate dependency coefficient ($\epsilon_{\dot{D}}|_0^{\dot{D}_{cal}}$) for a different number of beams.

It is clear from figures 2 and 3 that renormalization of the dose towards the maximum dose in the dose distribution has an enormous effect on the dose rate sensitivity. While one could conclude that it is better to use a renormalization of the dose distribution, it is important to realize that such a renormalization may also render the dosimetry insensitive for dose errors originating from the treatment.

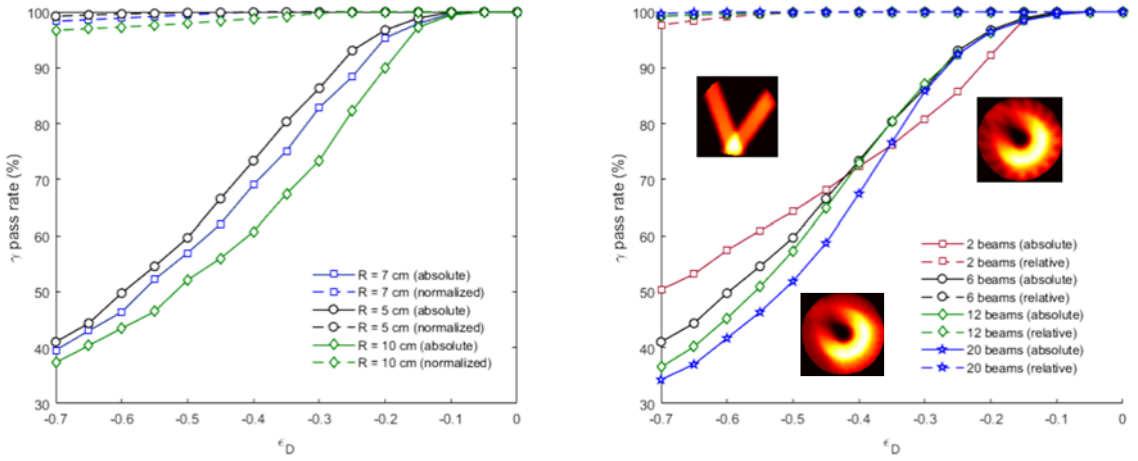

(a) **(b)**

Figure 4. Dependence of the gamma pass rate on the dose rate dependency coefficient for various phantom radii (a) and for different number of beams (b). The inset pictures are dose distributions for 2 beams, 12 beams and 20 beams.

Figure 3a and b demonstrate that the conclusions drawn from this study with respect to the dose rate dependency are relatively general irrespective of the phantom size and number of beams.

4. Conclusions

A fast dose calculation engine for homogenous irradiations was developed in Matlab to study the effect of a dose rate dependent dose response of radiation dosimeters.

Dose rate dependency of -10% does not affect the dose distribution significantly (gamma pass rate = 100%) and a dose rate dependency up to -15% results in a gamma pass rate of more than 98%. When the dose distribution is renormalized towards the maximum dose, a gamma pass rate of 99% is found for dose rate dependencies up to -40%. However, we do not recommend renormalization of the dose distribution as it may also obscure real treatment dose errors.

5. References

[1] De Deene Y *et al* 2006 *Phys. Med. Biol.* **51** 653-73
[2] Vandecasteele J *et al* 2011 *Phys. Med. Biol.* **56** 627-51
[3] Pappas E P *et al* 2017 *Radiother. Oncol* **123** S410
[4] De Deene Y *et al* 2015 *Phys. Med. Biol.* **60** 1543-63
[5] Jirasek A *et al* 2015 *Phys. Med. Biol.* **60** 4399-411
[6] De Gersem W *et al* 2001 *Int. J. Radiation Oncology Biol. Phys.* **51** 1371-88